Conservation of coactivator engagement mechanism enables small-molecule allosteric modulators

Andrew R. Henderson[a,b,1], Matthew J. Henley[a,b,1], Nicholas J. Foster[a,b], Amanda L. Peiffer[a,b], Matthew S. Beyersdorf[a,b], Kevon D. Stanford[a,c], Steven M. Sturlis[a], Brian M. Linhares[d], Zachary B. Hill[e], James A. Wells[e], Tomasz Cierpicki[b,d], Charles L. Brooks III[b,c,d], Carol A. Fierke[b,c], and Anna K. Mapp[a,b,c,2]

[a]Life Sciences Institute, University of Michigan, Ann Arbor, MI 48109; [b]Program in Chemical Biology, University of Michigan, Ann Arbor, MI 48109; [c]Department of Chemistry, University of Michigan, Ann Arbor, MI 48109; [d]Department of Biophysics, University of Michigan, Ann Arbor, MI 48109; and [e]Department of Pharmaceutical Chemistry, University of California, San Francisco, CA 94158

Edited by Benjamin F. Cravatt, The Scripps Research Institute, La Jolla, CA, and approved July 25, 2018 (received for review April 10, 2018)

Transcriptional coactivators are a molecular recognition marvel because a single domain within these proteins, the activator binding domain or ABD, interacts with multiple compositionally diverse transcriptional activators. Also remarkable is the structural diversity among ABDs, which range from conformationally dynamic helical motifs to those with a stable core such as a β-barrel. A significant objective is to define conserved properties of ABDs that allow them to interact with disparate activator sequences. The ABD of the coactivator Med25 (activator interaction domain or AcID) is unique in that it contains secondary structural elements that are on both ends of the spectrum: helices and loops that display significant conformational mobility and a seven-stranded β-barrel core that is structurally rigid. Using biophysical approaches, we build a mechanistic model of how AcID forms binary and ternary complexes with three distinct activators; despite its static core, Med25 forms short-lived, conformationally mobile, and structurally distinct complexes with each of the cognate partners. Further, ternary complex formation is facilitated by allosteric communication between binding surfaces on opposing faces of the β-barrel. The model emerging suggests that the conformational shifts and cooperative binding is mediated by a flexible substructure comprised of two dynamic helices and flanking loops, indicating a conserved mechanistic model of activator engagement across ABDs. Targeting a region of this substructure with a small-molecule covalent cochaperone modulates ternary complex formation. Our data support a general strategy for the identification of allosteric small-molecule modulators of ABDs, which are key targets for mechanistic studies as well as therapeutic applications.

Med25 | transcriptional coactivator | allosteric modulator | protein–protein interactions

Biophysical studies of complexes formed between the activator binding domains (ABDs) of transcriptional coactivators and their cognate activator binding partners suggest that modulating these functionally critical protein–protein interactions (PPIs) with small molecules is a formidable task (1). An excellent example of this is the ABD of the Mediator protein Med25, termed AcID (activator interaction domain; Fig. 1*A*) (2–4). As is standard for ABDs, AcID is a binding partner of a diverse array of transcriptional activators, including VP16, ATF6α (5), and the ETV/PEA3 activators (6, 7). Through these interactions, Med25 plays significant roles in the unfolded protein response and in oncogenesis, generating significant interest in small molecule modulators. However, data from NMR studies of AcID in complex with VP16 and ETV/PEA3 activators suggest that modulating these PPIs would not be trivial (2–4). The VP16 transcriptional activation domain contacts a surface of ∼1,800 Å^2 of AcID, wrapping around the topologically challenging β-barrel while also contacting two flanking helices. The transcriptional activation domain of the ETV/PEA3 member ERM interacts with one face of the β-barrel, a binding surface referred to as H1 that is ∼900 Å^2 in area (6, 7). The β-barrel core of AcID is unusual among ABDs, with helices more commonly observed, and raises the question of the role that the barrel might play in the molecular recognition of activators relative to the other substructures within AcID.

The observation that a portion of VP16 and ERM utilize the same H1 binding surface in AcID despite their distinct sequences suggests that conformational plasticity within the ABD could play a role in its molecular recognition capabilities and, ultimately, function. We considered the following criteria essential to support this model. First, each activator–AcID complex should be conformationally labile, with two or more conformation states energetically accessible. Second, two functionally similar binding sites such as H1 and H2 should be allosterically connected in a conformationally plastic domain. To test this model, we first identified ATF6α as an H2 binding site-specific ligand for AcID. Transient kinetic experiments with the activators VP16, ERM, and ATF6α revealed that in each case AcID exploits conformational lability to recognize the three distinct sequences in binary complexes as well as in ternary complexes. Molecular dynamics simulations highlighted the critical role that the flexible loops and helices play in the remodeling of one PPI surface, while also suggesting how these motions relate to the larger family of ABDs. Consistent with this

Significance

Transcriptional coactivators and their partner transcription factors have been labeled as intrinsically disordered, fuzzy, and undruggable. We propose that the identification of conserved mechanisms of engagement between coactivators and their cognate activators should provide general principles for small-molecule modulator discovery. Here, we show that the structurally divergent coactivator Med25 forms short-lived and dynamic complexes with three different transcriptional activators and that conformational shifts are mediated by a flexible substructure of two dynamical helices and flanking loops. Analogous substructures are found across coactivators. Further, targeting one of the flexible structures with a small molecule modulates Med25–activator complexes. Thus, the two conclusions of the work are actionable for the discovery of small-molecule modulators of this functionally important protein class.

Author contributions: A.R.H., M.J.H., N.J.F., A.L.P., M.S.B., S.M.S., C.L.B., C.A.F., and A.K.M. designed research; A.R.H., M.J.H., N.J.F., A.L.P., M.S.B., K.D.S., S.M.S., B.M.L., Z.B.H., and T.C. performed research; A.R.H., M.J.H., N.J.F., K.D.S., S.M.S., and Z.B.H. contributed new reagents/analytic tools; A.R.H., M.J.H., N.J.F., A.L.P., M.S.B., S.M.S., B.M.L., Z.B.H., J.A.W., T.C., C.L.B., C.A.F., and A.K.M. analyzed data; and A.R.H., M.J.H., and A.K.M. wrote the paper.

The authors declare no conflict of interest.

This article is a PNAS Direct Submission.

[1]A.R.H. and M.J.H. contributed equally to this work.

[2]To whom correspondence should be addressed. Email: amapp@umich.edu.

This article contains supporting information online at www.pnas.org/lookup/suppl/doi:10.1073/pnas.1806202115/-/DCSupplemental.

Published online August 20, 2018.

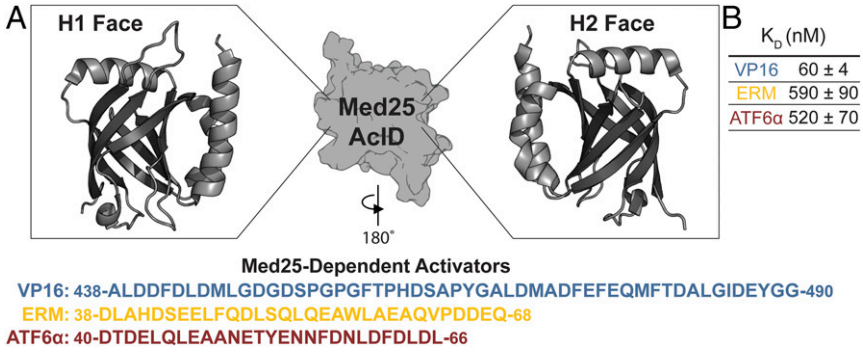

Fig. 1. Med25 AcID forms complexes with transcriptional activators of distinct sequences. (*A*) The AcID is the binding partner of a growing number of transcriptional activators and contains at least two binding surfaces, termed H1 and H2. The sequences of the transcriptional activation domains of the three Med25-dependent activators used in this study are shown below the protein structure (PDB ID code 2XNF). (*B*) Equilibrium dissociation constants for each of Med25 AcID–activator complexes, measured through fluorescence anisotropy experiments using fluorescein-labeled peptides. These values are the average of at least three independent measurements with the error indicated (standard deviation of the mean).

model, targeting one of the most dynamic regions of AcID with a small molecule cochaperone recapitulates the kinetic signatures of the native transcriptional activators. Taken together, these data suggest a conserved mechanism for transcriptional activators despite considerable structural divergence and that targeting the most dynamic regions of ABDs is a likely path forward for small molecule regulation of transcription through this important class of proteins.

Results and Discussion

ATF6α and ERM Bind to Opposite Faces of Med25 AcID. Separate NMR studies of AcID in complex with the transcriptional activation domains of VP16 and ERM suggest that the two activators both contact the H1 binding surface, with the significantly larger VP16 also interacting with the H2 surface (2–4). While several lines of evidence indicate that ATF6α interacts with Med25 AcID as part of its function (5), the binding site within the protein has not been established. We first measured the dissociation constants for each of the activators by fluorescence anisotropy experiments using fluorescein-tagged variants of VP16 (438–490), ERM (38–68), and ATF6α (40–66), and this revealed that ERM and ATF6α interact with comparable affinities (Fig. 1*B*) (2–5). To provide a direct comparison of the binding modes of the three activators and identify the binding site of ATF6α, we measured the chemical shift changes in each activator–AcID complex via ^{1}H, ^{15}N-HSQC NMR titration experiments, with VP16 (438–490), ERM (38–68), and ATF6α (40–66) in the presence of ^{15}N-labeled Med25 AcID (see *SI Appendix* for details of the design, synthesis, and characterization of each activator peptide).

The amide proton perturbation patterns measured for the activator–AcID complexes suggest a different binding mode for each of the three activators (Fig. 2). VP16 induced changes at both AcID binding surfaces, consistent with the tandem transcriptional activation domains within its sequence (*SI Appendix*, Figs. S13–S16). ERM binding predominantly lead to perturbations at residues on the H1 surface of AcID, in agreement with the model in which it preferentially interacts at that site (Fig. 2*A*

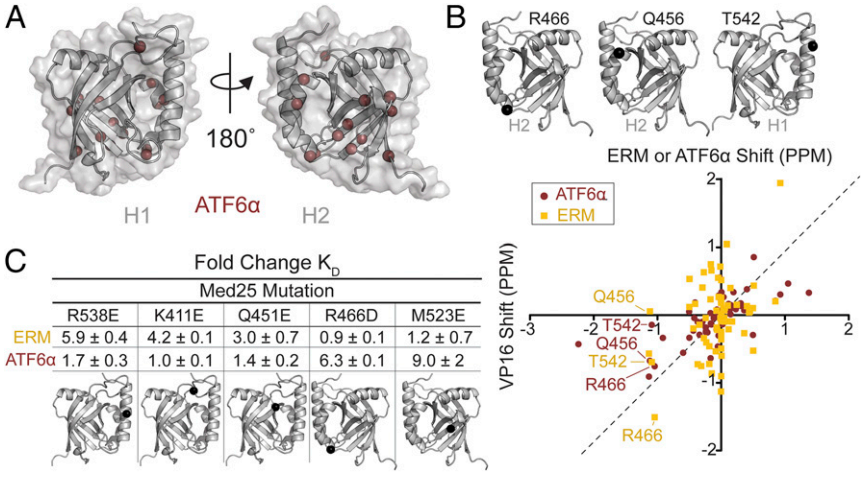

Fig. 2. ATF6α binds to the H2 surface of Med25 AcID. (*A*) Results of chemical shift perturbation experiments superimposed upon the Med25 AcID structure (PDB ID code 2XNF). Residues displaying chemical shift perturbation greater than 2 SD upon ATF6α binding are depicted in rust spheres. (*B*) Scatter plot illustrating correlations between the chemical shift perturbations (CSPs) of individual Med25 AcID residues from HSQC experiments with ERM, ATF6α, and VP16. The position of each maize square represents the CSP of an individual residue in Med25 AcID upon binding to ERM (*y* axis) and VP16 (*x* axis). Thus, squares along the dotted diagonal are residues that shift similarly in both ERM–AcID and VP16–AcID complexes. The same analysis for ATF6α is shown in rust circles. Specifically labeled are the positions of three residues that are on the H1 face of AcID (T542) and H2 face of AcID (R466, Q456), highlighting the distinct pattern of correlated CSPs for ERM and ATF6α, consistent with the model in which the two activators do not interact with the same binding site. Full CSP datasets for each of the three activator–Med25 AcID complexes are shown in *SI Appendix*. (*C*) Results of direct binding experiments with fluorescein-labeled activators and the indicated mutants of Med25 AcID as measured by fluorescence polarization expressed the fold change relative to the dissociation constant of each activator for the WT AcID. The indicated error is propagated from three independent dissociation constant measurements.

and *SI Appendix*, Figs. S17 and S18) (4, 6, 7). Key changes at residues K411, R538, and Q451, for example, were seen with both VP16 and ERM (Fig. 2*C*). In contrast, interaction with ATF6α lead to significant chemical shift changes on the H2 binding surface (Fig. 2*B* and *SI Appendix*, Figs. S19 and S20). ATF6α induced shifts of residues Q456, M470, and H474, which were also affected to varying degrees by VP16 and largely unaltered by ERM. Consistent with ATF6α and ERM interacting on opposing sides of AcID, mutations introduced on one or the other of the binding surfaces produced distinct effects (Fig. 2*C*). H1 mutations R538E, K411E, and Q451E inhibit ERM binding while ATF6α is largely unaffected. In contrast, H2 mutations R466D and M523E significantly inhibit ATF6α with minimal impact on ERM binding. Taken together, these data indicate that ATF6α binds on the H2 binding surface of Med25 AcID, opposite the site of ERM. Further, the distinct but overlapping chemical shift patterns observed upon binding of each of the activators to Med25 suggest several unique binding modes accommodated within AcID. This is analogous to helical activator binding domains such as GACKIX of CBP/p300, a three-helix bundle that contains at least two activator binding sites (8).

Activator–Med25 Complexes Are Conformationally Dynamic. Next, the underlying mechanistic features of activator–AcID complex formation were examined by determining association mechanisms of AcID with the TADs of VP16, ERM, and ATF6α using stopped-flow fluorescence spectroscopy. These kinetic experiments allow calculation of microscopic rate constants for association and dissociation, as well as forward and reverse rate constants for any conformational changes that happen during the binding process (9, 10). In practice, however, conformational changes involved in activator–coactivator interactions are often difficult to detect and quantify, and we thus chose the environmentally sensitive fluorophore 4-*N*,*N*-dimethylamino-1,8-napththalimide (4-DMN) as a fluorescence probe (Fig. 3*A*) (11, 12). This fluorophore was synthesized as a conjugate with β-alanine and incorporated at the amino terminus of these activators for subsequent experiments (synthetic protocols and characterization in *SI Appendix*).

Previous kinetic studies of helical coactivators revealed that complex formation with activators proceeds by fast association (k_{on}) and dissociation (k_{off}) rate constants (10, 13–17). Consistent with this observation, we found that activator–AcID complexes form with elevated k_{on} and k_{off} values, with k_{on} ranging between 300 and 1,100 $\mu M^{-1}{\cdot}s^{-1}$ and k_{off} ranging between 100 and 400 s^{-1} (Fig. 3). This behavior allows for activators to form tight interactions (K_D values 50–500 nM) with Med25 AcID that are short-lived, with activator residence times less than 10 ms. The k_{on} values are 1–2 orders of magnitude faster than most other activator-coactivator systems, likely a result of significant electrostatic contributions to binding (*SI Appendix*, Fig. S10), which can elevate association rate constants by several orders of magnitude (14, 15, 18).

At least one conformational change during the binding process was observed in all cases, with similar observed rate constants (k_{obs} = 10–40 s^{-1}) for each activator. The conformational change was determined to occur after the initial binding event by a

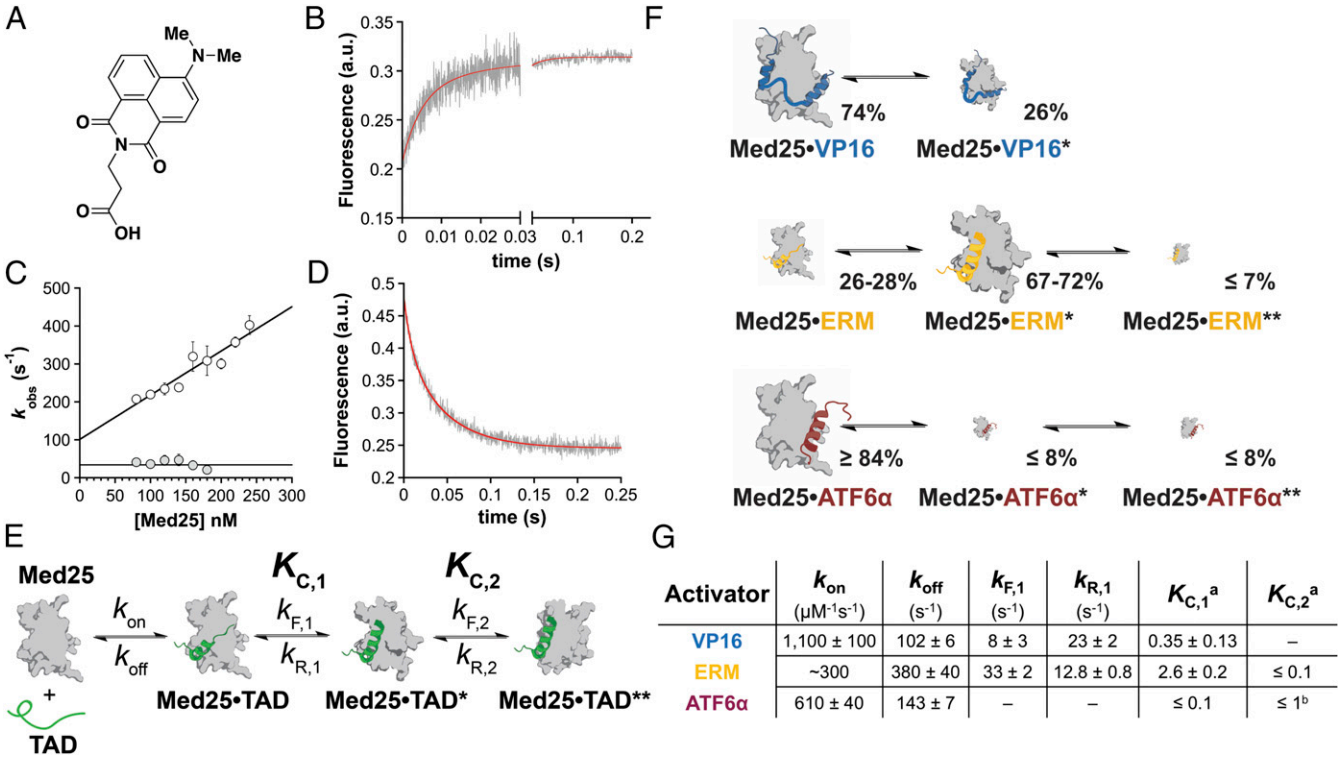

G

Activator	k_{on} ($\mu M^{-1}s^{-1}$)	k_{off} (s^{-1})	$k_{F,1}$ (s^{-1})	$k_{R,1}$ (s^{-1})	$K_{C,1}$[a]	$K_{C,2}$[a]
VP16	1,100 ± 100	102 ± 6	8 ± 3	23 ± 2	0.35 ± 0.13	–
ERM	~300	380 ± 40	33 ± 2	12.8 ± 0.8	2.6 ± 0.2	≤ 0.1
ATF6α	610 ± 40	143 ± 7	–	–	≤ 0.1	≤ 1[b]

Fig. 3. Transient kinetic experiments define minimal mechanism of activator–AcID complexation. (*A*) Structure of the fluorophore used in these experiments, 4-*N*,*N*-dimethylamino-1,8-napththalimide (4-DMN). (*B*) Representative kinetic trace of association experiment with DMN-VP16 and AcID. The red line is the fit to a two-step binding model (see *SI Appendix*, Figs. S2 and S3 for additional data). (*C*) Dependence of the two observed rate constants for the fast (white circles) and slow (gray circles) kinetic phases on the concentration of AcID for association experiments of VP16 with AcID. (*D*) Sample kinetic trace of a dissociation experiment in which unlabeled VP16 was added in excess to preformed DMN-VP16–AcID. (*E*) General kinetic mechanism for TAD–AcID complex formation as determined by these experiments for all activators. Microscopic equilibrium constants ($K_{C,n}$) are defined as the ratio of the respective forward and reverse rate constants. (*F*) Representation of equilibrium population distributions of bound states, calculated from equilibrium constants in 3G. Transparency of each state is scaled according to the indicated percentage population. When one equilibrium constant is too small to measure, the values are given as ranges. (*G*) Measured kinetic and equilibrium constants for all of the activators. Kinetic constants $k_{F,2}$ and $k_{R,2}$ are unable to be reliably calculated. a, The conformational change equilibrium constant is too small to be measured with precision. b, The overall equilibrium constant from Med25–ATF6a to Med25–ATF6a** is estimated to be ≤0.1 based on the limits of precision of our experiments, thus given that $K_{C,1} \leq 0.1$, $K_{C,2}$ must be ≤1.

combination of global fitting in Kintek Explorer and an "inverted" association experiment (see *SI Appendix* for additional details, including *SI Appendix*, Figs. S3 and S5*F*) (19, 20). Importantly, the equilibrium constant of this conformational change ($K_{C,1}$) varied significantly across activators (Fig. 3*F*). For the activator VP16, which binds both sites simultaneously, the initial bound state was somewhat more favorable ($K_{C,1}$ = 0.35 ± 0.13). In contrast, the activators ERM and ATF6α, which bind to opposite sites of AcID, had $K_{C,1}$ values that were significantly larger and smaller than VP16 (438–490), respectively ($K_{C,1}$ = 2.6 ± 0.2 and <0.1). This range of $K_{C,1}$ values is not unusual for activator-coactivator association mechanisms; we have previously observed this behavior with activator–Med15 complexes, where $K_{C,1}$ values positively correlated with transcriptional output (10, 21, 22). A second conformational change for ERM and ATF6α that was slower (k_{obs} = 2–6 s^{-1}) was also detected in these experiments and had equilibrium constants that were too small to quantify reliably. Global fitting of the kinetic traces suggested this conformational change happens after the primary conformational change.

Some structural insight regarding the primary conformational change of the ERM–AcID complex was gained from the $^{1}H,^{15}N$ HSQC titration of ERM with AcID, as many AcID residues display slow and intermediate exchange behavior in this complex (*SI Appendix*, Fig. S25). Specifically, the intermediate exchange behavior points to conformational exchange on the millisecond timescale ($\Delta\nu$ = 30–180 s^{-1}), consistent with the value of the exchange rate constant measured in the kinetics experiments (45 s^{-1}). Thus, inspecting the residues that display signal broadening shows that this conformational change involves residues at both sites (*SI Appendix*, Fig. S25), including many residues on the flexible loops and all three helices. Taken together, the NMR and kinetic data point to a mode of interaction where Med25 AcID forms conformationally unique complexes with its activator interaction partners. While these activators bind to Med25 with similar affinities, they each have different kinetic signatures characterized by a conformational change after binding that extends throughout the AcID structure. Finally, all of these complexes can be described as "fuzzy"; at equilibrium, each complex contains multiple populated conformational substates that are separated by low energy barriers (23).

The H1 and H2 Binding Sites Are in Allosteric Communication. The presence of two binding sites that engage with distinct activators raises the question whether AcID contains an allosteric network linking the two sites to permit cooperative formation of specific activator–AcID ternary complexes. The prototypical case of allostery in ABD–activator complex formation is the GACKIX motif in CBP/p300 (10, 13, 15, 24, 25). In this example, the "signature" of allosteric communication is reduction of the k_{off} of an activator when another activator is bound at the allosteric site, with the k_{on} largely unaffected. Thus, for AcID, we measured dissociation rate constants as a primary method to detect allosteric communication.

We first looked to use the VP16 TAD as a model system; the two halves represent individual interaction motifs that bind separate sites, and when employed in trans, it would be expected that they could be used to dissect communication between AcID sites. However, when separated, the two VP16 halves lose 10- to 15-fold affinity and display poor selectivity for one binding site over another (*SI Appendix*, Fig. S12), which is not surprising given the topological similarity between the two binding sites of AcID and the high sequence homology between the two VP16 activator motifs. This reduced selectivity significantly complicates data interpretation as the presence of multiple distinct ternary complexes can mask allosteric effects. To address this, we took advantage of a distinguishing feature between the AcID binding sites, the presence of two solvent-exposed cysteine residues (C497 and C506) within the H1 site, which were then employed to tether the relevant VP16 fragment to that site via a disulfide. Tethering experiments with a library of disulfide-containing point mutations of the H1-targeting portion of VP16, VP16 (438–454), were carried out with AcID, and the G450C mutation led to 100% formation of a disulfide bond with the C506 residue of AcID, even under stringent conditions. Biophysical characterization of the covalent complex (*SI Appendix*, Figs. S9, S11, and S21) indicates that it recapitulates the features of the noncovalent complex (26). Consistent with the hypothesis of allosteric communication, multiple chemical shifts corresponding to residues in the H2 site are perturbed in the $^{1}H,^{15}N$ HSQC spectrum (*SI Appendix*, Figs. S21 and S22). In contrast, the introduction of cysteine to the H2 surface at a variety of positions produced mutants with a high aggregation propensity, rendering them unsuitable for Tethering and binding studies.

With this tool in hand, two separate 4-DMN–labeled probes that interact with the H2 binding site, VP16 (467–488) and ATF6α, were used to assess changes in ternary complex formation upon occupancy of the H1 site of AcID (Fig. 4*A*). As a complement to the covalent system, ERM was also employed as a noncovalent H1 partner in a separate set of experiments due to its greater apparent selectivity for the H1 binding surface. With VP16 $(438–454)_{G450C}$ tethered at the H1 site, the k_{off} value of the VP16 (467–488) ligand was reduced by 20% (Fig. 4*B*). The corresponding value for the ATF6α probe was reduced by ∼10%, although this did not reach statistical significance (P = 0.1). Consistent with our hypothesized model, k_{on} for ATF6α was unchanged; we were unable to measure VP16 (467–488) k_{on} due to a very high k_{off} value. When ERM was bound to the H1 site, k_{off} for VP16 (467–488) displayed a similar 20% reduction, while the

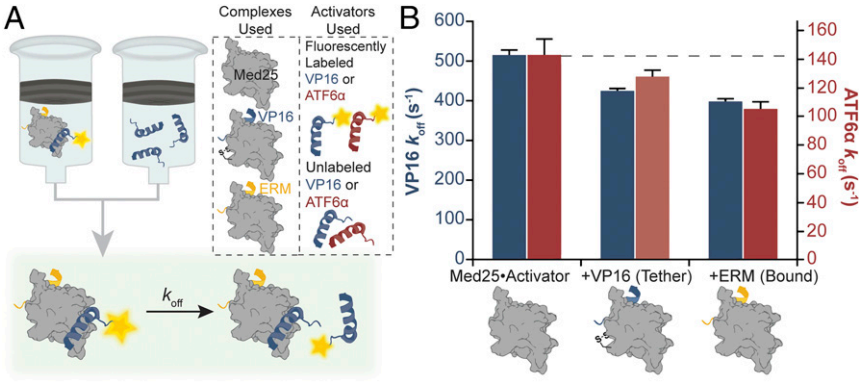

Fig. 4. Dissociation experiments reveal allosteric communication between two binding sites. (*A*) Schematic of the experiment. (*B*) Comparison of k_{off} for VP16 (467–488) (blue bars) for Med25 AcID, Med25 AcID with VP16 $(438–454)_{G450C}$ covalently Tethered, and Med25 AcID with ERM prebound; the red bars summarize data from analogous experiments with ATF6α. The values shown are the average of 2–3 independent experiments with the indicated errors (SD). All changes from the binary complex were statistically significant (P < 0.01), except for the Tethered complex bound to ATF6α (transparent bar).

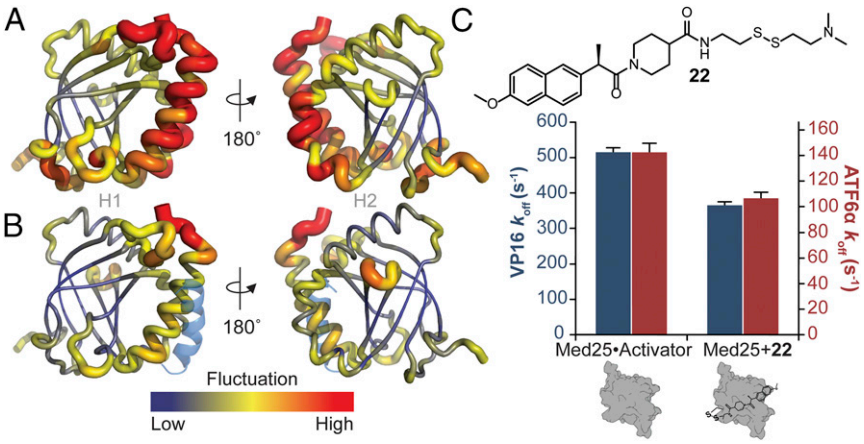

Fig. 5. Emerging structural model for AcID–activator complex formation. (*A* and *B*) The NMR coordinates for Med25 AcID (PDB ID code 2XNF) (2) were used to construct the initial structure of Med25 in CHARMM using the Multiscale Modeling Tools for Structural Biology. For *B*, VP16 (438–454) G450C was constructed in CHARMM as a helical peptide, which was then patched in CHARMM to Med25 C506 through the formation of a disulfide bond at C506 (transparent blue helix). Using GBSW implicit solvent, temperature replica exchange was implemented using the CHARMM22 force field (32). The RMSFs were calculated for each Med25 AcID residue by overlaying Cα atoms for all of the coordinate files produced from the simulations. The coloring correlates with the degree of dynamical behavior of each region. (*C*) Structure of chemical cochaperone **22** obtained from a Tethering screen. The bar graph is a comparison of k_{off} for VP16 (467–488) (blue bars) for Med25 AcID or Med25 AcID with **22** covalently Tethered; the red bars summarize data from analogous experiments with ATF6α. The values shown are the average of 2–3 independent experiments with the indicated errors (SD).

ATF6α k_{off} value was reduced by 25%.* Taken together, the data demonstrates that the two binding sites of Med25 AcID are allosterically linked, and the mechanism of allosteric communication (reduction of k_{off}) is analogous to that of the GACKIX motif (13, 15). These measured cooperativity values (~1.3) are similar to values previously measured for GACKIX, which are in the range of 1.4–2.2 for most ternary complexes, but in certain cases, are as high as 18. We expect as more Med25 binding partners are reported and characterized these cooperativity factors will also vary significantly for different ternary complexes (27).

A Covalent Cochaperone Recapitulates Allosteric Changes. We have previously demonstrated that prototypical conformationally dynamic coactivators such as GACKIX can be allosterically modulated by covalent cochaperones (13, 28); these can be rapidly identified with the covalent fragment discovery method of Tethering. In the GACKIX case, engagement with the most dynamic sites within the coactivator lead to the most effective cochaperones. To identify such regions within Med25 AcID suitable for chemical cochaperone discovery, all-atom molecular dynamics simulations were carried out using implicit solvent models (GBSW) and with temperature replica exchange in CHARMM (29–32). Simulations were performed on both unbound Med25 AcID and a model of this protein in which the VP16 $(438–454)_{G450C}$ is tethered at C506. To identify the substructures most stabilized upon binding, the root-mean-square fluctuations (RMSF) for each residue were calculated from the resulting trajectories (Fig. 5 *A* and *B*). In these figures, the line color reflects the range of motion of each residue. In the unbound structure (Fig. 5*A*), the β-barrel core is relatively static whereas the loops and helices framing the two binding sites show particular mobility. The presence of VP16 (438–454) significantly alters the extent of motion (Fig. 5*B*). Particularly notable is that the upper loop on the H1 binding surface (residues 409–424 of Med25) appears to strongly interact with VP16. Supporting this model is the effect of mutations within this region on another H1 binding activator, ERM; a K411E mutation, for example, resulted in fourfold weaker ERM binding (Fig. 2*C*). The loop at the lower portion of this binding interface (residues 435–446) is also significantly altered upon interaction with VP16 and, again, interaction with H1 face-targeting ligands such as ERM is altered upon mutation at this site. The helices flanking the H1 binding surface also undergo significant stabilization upon binding, suggesting that they also play an important role in the defining the binding site. An analysis of RMSFs of residues in Med25 AcID unbound to any ligand reveals that the most dynamical regions of the protein are indeed the loops, with significant motion in the flanking helices as well, consistent with the preliminary structural model (2, 3).

The two solvent-accessible cysteines (C497 and C506) in Med25 AcID are adjacent to regions that are predicted to be the most mobile in the preliminary structural model outlined above and that are most affected by activator binding. Thus, a Tethering screen of Med25 AcID utilizing a 1,600-member library was carried out using standard methods (33, 34). This experiment identified cochaperone **22** as a molecule that covalently labels C506 in Med25 AcID with high efficiency (*SI Appendix*, Fig. S23). We tested the allosteric effects of the Tethered compound **22** using transient kinetics analogous to the experiments of Fig. 4. Similar to the effects of natural activator ligands, the values of k_{off} for both labeled activators were reduced by 25% in the presence of **22** while k_{on} was unaffected. Thus, even a fragment molecule can recapitulate the key binding features of a natural activator despite considerable differences in size. This suggests that Med25 AcID will be druggable through the targeting of its most dynamic regions, despite its large binding surfaces. Particularly given our prior success with a similarly dynamic but structurally distinct ABD from CBP/p300, this appears to be a general strategy for the discovery of small molecule modulators of transcriptional coactivators.

Conclusions

Despite having a seemingly simple function, formation of one or more protein–protein interactions with transcriptional activators, the activator binding domain of a coactivator must be able to form PPIs in binary and ternary complexes that are both specific and short-lived to facilitate appropriate assembly of the transcriptional machinery and initiation. An additional complicating factor is that a single ABD is typically the cognate binding partner for tens of different activators, requiring a significant degree of structural mobility in the ABD to accommodate this diversity. This mobility likely corresponds to local folding-like transitions; it not only allows the binding interfaces to morph into unique conformations as part

*In contrast to AcID covalently tethered to $VP16(438-454)_{G450C}$, when AcID is noncovalently bound to ERM the apparent k_{on} value for ATF6α is decreased by 30%. However, analysis of the raw kinetic traces strongly indicates that this change is due to a small fraction of ERM binding to the H2 site, and it is likely that in the absence of this masking effect k_{on} is relatively unchanged. See *SI Appendix* for data and discussion.

of binding different activators, but underlies the allosteric interactions between different binding sites in an individual domain (35, 36). Therefore, the "important" molecular recognition elements should be the most mobile regions, which is in line with our results shown here with Med25 AcID. Despite the large surface area of the core β-barrel that is used for interacting with activators, it is changes in the flanking loops and helices that enable accommodation of the distinct cognate ligands. Further, the emerging structural model suggests that it is also these regions that are responsible for allosteric communication between the two binding surfaces. Consistent with this model, engagement of one of the most mobile regions with a covalent cochaperone indeed alters binding at the opposing sites. Importantly, this suggests that this seemingly "undruggable" protein is likely targetable by allosteric small molecules (via our targeting strategy), as should transcriptional coactivators more broadly. Given the central role that many coactivators play in human disease, this will be a critical advance. Further, since the first structural reports of AcID, the identity of activator and coactivator binding partners of Med25 has expanded (27), and the molecular recognition model outlined here indicates that cooperative binding of Med25 to activators and/or coactivators such as CBP may be a key regulatory mechanism.

Methods

Protein Expression and Purification. The Med25 AcID expression plasmid pET21b-Med25(394-543)-His_6 was generously provided by Patrick Cramer, Max Planck Institute for Biophysical Chemistry, Göttingen, Germany (2). Variants of pET21b-Med25(394-543)-His_6 were prepared using site-directed mutagenesis and expressed in *Escherichia coli* Rosetta cells. Protein identity was confirmed by mass spectrometry using an Agilent Q-TOF. Protein for NMR experiments was prepared with either ^{15}N or $^{15}N,^{13}C$ labeling. M9 minimal media was supplemented with Bioexpress (6 mL/L) and 1 g/L $^{15}NH_4Cl$ or 1 g/L $^{15}NH_4Cl$ and ^{13}C D-glucose for ^{15}N and $^{15}N,^{13}C$ Med25 AcID, respectively. Protein identity was confirmed using an Agilent Q-TOF.

Peptide Synthesis. The peptides used in these studies were prepared following standard FMOC solid-phase synthesis methods on a Liberty Blue Microwave Synthesizer (CEM). Additional details, including analytical HPLC traces, can be found in the *SI Appendix*.

NMR Analyses of Activator–AcID Complexes. $^{1}H,^{15}N$ HSQC experiments of activator–AcID complexes were performed on a Bruker Avance III 600 MHz spectrometer equipped with a cryogenic probe at 30 °C. Titrations were conducted with Med25 AcID (20 mM $NaPO_4$, 150 mM NaCl, pH 6.5, 5% D_2O) at 50 μM, and acetylated peptides were added at 0, 0.2, 0.5, 0.8, 1.1, 2, and 3 eq with a 2% final DMSO concentration. Control spectra were obtained with Med25 AcID and DMSO only. Tethered activator–AcID complexes were prepared as previously described (26). Data processing and visualization was performed using NMR Pipe and Sparky (37).

Kinetic Analyses of Activator–AcID Complexes. Stopped-flow kinetic assays were performed as described (13). The 4-DMN fluorophore was excited at 440 nm with emission monitored at wavelengths >510 nm, using a long-pass filter (Corion). Additional details and discussion can be found in *SI Appendix*.

ACKNOWLEDGMENTS. Financial support for this work was received from NIH Grant 3R01 GM65530 (to A.K.M.) and Leukemia and Lymphoma Society Grant 1340-17 (to T.C.), and N.J.F. was supported by NIH Fellowship GM65530-S2. M.S.B. and M.J.H. acknowledge fellowships from the Department of Education (Graduate Assistance in Areas of National Need).

1. Mapp AK, Pricer R, Sturlis S (2015) Targeting transcription is no longer a quixotic quest. *Nat Chem Biol* 11:891–894.
2. Vojnic E, et al. (2011) Structure and VP16 binding of the mediator Med25 activator interaction domain. *Nat Struct Mol Biol* 18:404–409.
3. Milbradt AG, et al. (2011) Structure of the VP16 transactivator target in the Mediator. *Nat Struct Mol Biol* 18:410–415.
4. Bontems F, et al. (2011) NMR structure of the human mediator MED25 ACID domain. *J Struct Biol* 174:245–251.
5. Sela D, et al. (2013) Role for human mediator subunit MED25 in recruitment of mediator to promoters by endoplasmic reticulum stress-responsive transcription factor ATF6α. *J Biol Chem* 288:26179–26187.
6. Verger A, et al. (2013) The mediator complex subunit MED25 is targeted by the N-terminal transactivation domain of the PEA3 group members. *Nucleic Acids Res* 41: 4847–4859.
7. Landrieu I, et al. (2015) Characterization of ERM transactivation domain binding to the ACID/PTOV domain of the mediator subunit MED25. *Nucleic Acids Res* 43: 7110–7121.
8. Dyson HJ, Wright PE (2016) Role of intrinsic protein disorder in the function and interactions of the transcriptional coactivators CREB-binding protein (CBP) and p300. *J Biol Chem* 291:6714–6722.
9. Johnson KA (1986) Rapid kinetic analysis of mechanochemical adenosinetriphosphatases. *Methods Enzymol* 134:677–705.
10. Wands AM, et al. (2011) Transient-state kinetic analysis of transcriptional activator·DNA complexes interacting with a key coactivator. *J Biol Chem* 286:16238–16245.
11. Shammas SL, Crabtree MD, Dahal L, Wicky BI, Clarke J (2016) Insights into coupled folding and binding mechanisms from kinetic studies. *J Biol Chem* 291:6689–6695.
12. Loving G, Imperiali B (2008) A versatile amino acid analogue of the solvatochromic fluorophore 4-N,N-dimethylamino-1,8-naphthalimide: A powerful tool for the study of dynamic protein interactions. *J Am Chem Soc* 130:13630–13638.
13. Wang N, Lodge JM, Fierke CA, Mapp AK (2014) Dissecting allosteric effects of activator-coactivator complexes using a covalent small molecule ligand. *Proc Natl Acad Sci USA* 111:12061–12066.
14. Shammas SL, Travis AJ, Clarke J (2013) Remarkably fast coupled folding and binding of the intrinsically disordered transactivation domain of cMyb to CBP KIX. *J Phys Chem B* 117:13346–13356.
15. Shammas SL, Travis AJ, Clarke J (2014) Allostery within a transcription coactivator is predominantly mediated through dissociation rate constants. *Proc Natl Acad Sci USA* 111:12055–12060.
16. Gianni S, Morrone A, Giri R, Brunori M (2012) A folding-after-binding mechanism describes the recognition between the transactivation domain of c-Myb and the KIX domain of the CREB-binding protein. *Biochem Biophys Res Commun* 428:205–209.
17. Dogan J, Schmidt T, Mu X, Engström Å, Jemth P (2012) Fast association and slow transitions in the interaction between two intrinsically disordered protein domains. *J Biol Chem* 287:34316–34324.
18. Schreiber G, Fersht AR (1996) Rapid, electrostatically assisted association of proteins. *Nat Struct Biol* 3:427–431.
19. Johnson KA, Simpson ZB, Blom T (2009) Global kinetic explorer: A new computer program for dynamic simulation and fitting of kinetic data. *Anal Biochem* 387:20–29.
20. Gianni S, Dogan J, Jemth P (2014) Distinguishing induced fit from conformational selection. *Biophys Chem* 189:33–39.
21. Brüschweiler S, et al. (2009) Direct observation of the dynamic process underlying allosteric signal transmission. *J Am Chem Soc* 131:3063–3068.
22. Sugase K, Dyson HJ, Wright PE (2007) Mechanism of coupled folding and binding of an intrinsically disordered protein. *Nature* 447:1021–1025.
23. Tompa P, Fuxreiter M (2008) Fuzzy complexes: Polymorphism and structural disorder in protein-protein interactions. *Trends Biochem Sci* 33:2–8.
24. Ernst P, Wang J, Huang M, Goodman RH, Korsmeyer SJ (2001) MLL and CREB bind cooperatively to the nuclear coactivator CREB-binding protein. *Mol Cell Biol* 21: 2249–2258.
25. Law SM, Gagnon JK, Mapp AK, Brooks CL, 3rd (2014) Prepaying the entropic cost for allosteric regulation in KIX. *Proc Natl Acad Sci USA* 111:12067–12072.
26. Sadowsky JD, et al. (2011) Turning a protein kinase on or off from a single allosteric site via disulfide trapping. *Proc Natl Acad Sci USA* 108:6056–6061.
27. Currie SL, et al. (2017) ETV4 and AP1 transcription factors form multivalent interactions with three sites on the MED25 activator-interacting domain. *J Mol Biol* 429: 2975–2995.
28. Wang N, et al. (2013) Ordering a dynamic protein via a small-molecule stabilizer. *J Am Chem Soc* 135:3363–3366.
29. Im W, Lee MS, Brooks CL, 3rd (2003) Generalized born model with a simple smoothing function. *J Comput Chem* 24:1691–1702.
30. Chen J, Im W, Brooks CL, 3rd (2006) Balancing solvation and intramolecular interactions: Toward a consistent generalized born force field. *J Am Chem Soc* 128: 3728–3736.
31. MacKerell AD, et al. (1998) All-atom empirical potential for molecular modeling and dynamics studies of proteins. *J Phys Chem B* 102:3586–3616.
32. Sugita Y, Okamoto Y (1999) Replica-exchange molecular dynamics method for protein folding. *Chem Phys Lett* 314:141–151.
33. Erlanson DA, et al. (2000) Site-directed ligand discovery. *Proc Natl Acad Sci USA* 97: 9367–9372.
34. Erlanson DA, Wells JA, Braisted AC (2004) Tethering: Fragment-based drug discovery. *Annu Rev Biophys Biomol Struct* 33:199–223.
35. Hilser VJ, Thompson EB (2007) Intrinsic disorder as a mechanism to optimize allosteric coupling in proteins. *Proc Natl Acad Sci USA* 104:8311–8315.
36. Schrank TP, Bolen DW, Hilser VJ (2009) Rational modulation of conformational fluctuations in adenylate kinase reveals a local unfolding mechanism for allostery and functional adaptation in proteins. *Proc Natl Acad Sci USA* 106:16984–16989.
37. Delaglio F, et al. (1995) NMRPipe: A multidimensional spectral processing system based on UNIX pipes. *J Biomol NMR* 6:277–293.